

Fatigue crack growth and remaining life estimation of AVLB components

Hung-Liang (Roger) Chen[†] and Jeong-Hoon Choi[‡]

Department of Civil & Environmental Engineering, West Virginia University, Morgantown, WV 26506, USA

(Received November 9, 2005, Accepted April 6, 2006)

Abstract. The fatigue cracks initiate and propagate in the Armored Vehicle Launch Bridge (AVLB) components, especially like the splice doubler angle, splice plate, and bottom chord, due to the cyclic loading by repeated AVLB-launchings and tank-crossings. In this study, laboratory fatigue tests were conducted on six aluminum 2014-T6, four aluminum 7050-T76511, and four ASTM A36 steel compact-tension specimens to evaluate the crack growth behavior of the materials used for the components. The experimental results provide the relationship (*Paris Law*) between crack growth rate, da/dn , and stress intensity range, ΔK , whose material dependent constants C and m can later be used in the life estimation of the components. Finite Element Method (FEM) was used to obtain the stress intensity factor, K , of the components with cracks. Because of the complexity of loading conditions and component geometry, several assumptions and simplifications are made in the FEM modeling. The FEM results, along with the results obtained from laboratory fatigue tests, are then utilized to estimate critical crack length and remaining life of the components.

Keywords: AVLB sub-components; fatigue crack growth; stress intensity factor; finite element method; remaining fatigue-life estimation.

1. Introduction

The Armored Vehicle Launch Bridge (AVLB), which has been used in the field since the early 1960's, is a folding scissors-type bridge and is a component of M48 or M60 launcher, riding atop the vehicle. The AVLB itself is constructed primarily of aluminum alloy and is rated for normal crossing of Military Load Classification (MLC) 60 loads at a maximum span of 18.3 m (60 ft.) (Cho 1994). According to the Preventive Maintenance Checks and Services (PMCS) in the engineering technical manual by the department of the U.S. Army (1990), the AVLB suffers various types of damage to its components, such as fatigue, shear, bending damages, etc. In general, these types of damage occur simultaneously in a component, leading to difficulty of analyzing component failure.

The splice doubler angle, the splice plate, and the bottom chord are reported especially susceptible to fatigue damage. These components are subjected to cyclic loadings by repeated AVLB-launchings and tank-crossings over the bridge. The application of cyclic loading to the components, especially

[†] Professor, Corresponding author, E-mail: hchen@wvu.edu

[‡] Graduate Research Assistant, E-mail: jchoi1@mix.wvu.edu

those with defects, causes cracks to initiate and subsequently propagate. These cracks need to be detected and repaired before they rapidly grow to reach their critical stage of propagation; otherwise, the failure of components can occur, which may result in the failure of the entire AVLB. Aluminum 2014-T6 has been used to manufacture these three components of the AVLB located at West Virginia University (WVU). Additionally, aluminum 7050-T76511 has been used for the splice doubler angle and bottom chord of the upgraded AVLB (MLC 70), and ASTM A36 steel for the splice plate of the upgraded AVLB. This study is focused only on these components and materials.

During the fatigue cracking process, the stress intensity factor, K , can be used to indicate the stress levels of the components. There are many factors contributing to the estimation of the remaining life of the components. These include the number of cycles required to initiate a crack, the critical crack length, the geometry of the component, the applied stress range and its loading rate, the effect of an aggressive environment on fatigue crack growth rate, and the remaining residual stresses (Chen and Fultineer 1996). Several previous studies have been conducted to present the fatigue crack growth behavior of various aluminum alloys (Clark and Wessel 1967, Crooker 1971, Gan and Weertman 1981, Kermandidis and Pantelakis 2001) and steels (Barsom 1971, Parry *et al.* 1972, James 1972, Roessle and Fatemi 2000). Particularly, several articles are written pertaining to the fatigue crack propagation in complicated geometric features. The fatigue crack propagation in a prismatic specimen having a square cross section and a drilled hole at its center has been investigated (Dhondt 2005). The crack is assumed to initiate from the outer surface and propagate towards the hole under the tensile forces applied at both ends of the specimen. Its numerical analysis reveals that as soon as the crack crosses a discontinuity (hole), it results in locally increasing K values and accelerated crack propagation. Cracks often initiate from the mechanical joints, such as bolted, riveted, or pinned joints, because of the stress concentration and contact pressure, and the fatigue crack growth path from the mechanical joints has been predicted by the maximum tangential stress criterion using the Mode I and Mode II stress intensity factors (Heo and Yang 2002). The fatigue crack propagation, especially in the riveted lab-joint, has been studied as well, and it reveals that the fatigue crack appears to initiate, in most cases, from the locations around the rivet-hole where the highest tensile concentration occurs depending on the amount of fastener clamping and level of applied load (Iyer *et al.* 2005).

The objective of this study is to estimate the critical crack length and remaining life of the three critical sub-components of the AVLB, and to establish acoustic emission (AE) signal characteristics of the materials used for the components; however, due to the length restriction of this paper, the AE part of this study has been discussed in another article (Chen and Choi 2004). The results of this study will eventually help to develop a damage assessment expert system, which can be used to determine the structural integrity of the AVLB. In addition, the effect of the loading parameters, such as loading frequency and ratio, on the crack growth rate of different materials is investigated in this study.

The scope of this paper includes the fracture mechanics approach to conduct laboratory fatigue tests and Finite Element Method (FEM) to obtain the stress intensity factor, K , of the components with cracks, based on Linear Elastic Fracture Mechanics (LEFM). The FEM results, along with the results obtained from laboratory fatigue tests on aluminum 2014-T6, are then utilized to evaluate the critical crack length and remaining life of the AVLB sub-components. The information used in modeling is based on an AVLB located at WVU. Two more materials, aluminum 7050-T76511 and ASTM A36 steel, which are used for the critical components of an upgraded AVLB, are also fatigue-tested in the laboratory. The compact-tension specimen is adopted for the fatigue tests of each material. The experiments are conducted at the load ratios, R , of 0.1 and 0.5.

2. Experiments

2.1 Preparation of specimen

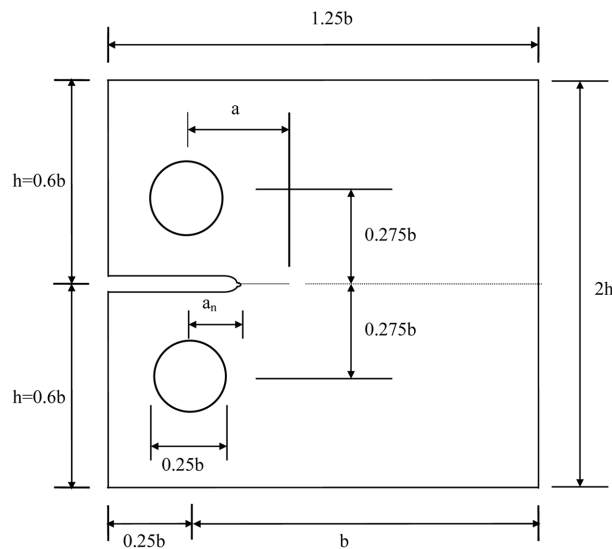
Six aluminum 2014-T6, four aluminum 7050-T76511, and four ASTM A36 steel compact-tension specimens were prepared in accordance with the standard dimensions in the standard ASTM E647-95. All similar specimens were cut by following the L-T combination of crack plane and growth direction in a rectangular section of the material. The thickness of the specimen for each material type was the same as that of the corresponding AVLB component. Table 1 lists the mechanical properties of these materials, and Fig. 1 illustrates the specimen dimensions. Each specimen was prepared introducing a machined notch, which facilitates obtaining ideally sharp cracks. The details

Table 1 Mechanical properties of materials tested

Material	Mechanical properties				
	E (Pa)	G (Pa)	ν	σ_o (Pa)	K_{Ic} (MPa \sqrt{m})
Aluminum 2014-T6	72.4×10^9	27.6×10^9	0.33	413.7×10^6	25 ⁽¹⁾
Aluminum 7050-T76511	71.0×10^9	26.9×10^9	0.33	517.1×10^6	44 ⁽¹⁾
ASTM A36 Steel	200×10^9	77.2×10^9	0.29	358.5×10^6	99 ⁽²⁾

⁽¹⁾ASM HANDBOOK 1990.

⁽²⁾Hamstad and McColskey 1999.



	Width (b ; mm)	Thickness (t ; mm)
2014-T6 Specimen	101.6	9.525
7050-T76511 Specimen	98.425	6.35
ASTM A36 Specimen	101.6	6.35

Fig. 1 Standard compact-tension specimen

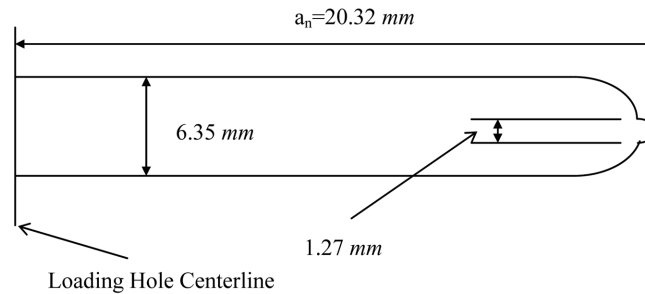


Fig. 2 Details of notch and notch tip

Table 2 Initial crack length and loading specifications for each specimen (AL1: Aluminum 2014-T6, AL2: Aluminum 7050-T76511, ST: ASTM A36 steel)

Specimen	Material	Initial crack length (mm)	P_{min}/P_{max} (kN)	Load ratio, R	Loading frequency (Hz)
AL1#1	Aluminum 2014-T6	30.7	0.534/5.34	0.1	1.5
AL1#2	Aluminum 2014-T6	27.9	0.534/5.34	0.1	1.5
AL1#3	Aluminum 2014-T6	27.7	0.534/5.34	0.1	4
AL1#4	Aluminum 2014-T6	41.2	2.67/5.34	0.5	1.5
AL1#5	Aluminum 2014-T6	30.2	2.67/5.34	0.5	1.5
AL1#6	Aluminum 2014-T6	31.8	2.67/5.34	0.5	4
AL2#1	Aluminum 7050-T76511	31.4	0.490/4.90	0.1	1.5
AL2#2	Aluminum 7050-T76511	26.8	0.490/4.90	0.1	1.5
AL2#3	Aluminum 7050-T76511	27.8	2.45/4.90	0.5	1.5
AL2#4	Aluminum 7050-T76511	27.6	2.45/4.90	0.5	1.5
ST#1	ASTM A36 Steel	26.9	0.490/4.90	0.1	4
ST#2	ASTM A36 Steel	27.0	0.490/4.90	0.1	4
ST#3	ASTM A36 Steel	28.2	3.11/6.22	0.5	4
ST#4	ASTM A36 Steel	27.2	3.11/6.22	0.5	4

of the notch and its tip are given in Fig. 2. In addition, the nomenclature to identify each specimen is shown in Table 2.

2.2 Instrumentation and experimental procedures

All specimens were tested in the load-controlled mode of an INSTRON model 1331, which is a closed-loop loading system with a load cell enabled to sustain the maximum load capacity of 97.86 kN (22 kips). The specimens were subjected to cyclic tension-tension loading in the sinusoidal wave shape.

Two different crack propagation gages, the TK-09-CPA02-005/DP and TK-09-CPC03-003/DP (Measurements Group, INC), were used to monitor the crack propagation in the specimens during this study. Both consisted of 20 resistor strands connected in parallel. The breaking of strands due to the crack propagation caused stepped increases in resistance of the gage. These increases in

resistance then caused voltage increases in the parametric for the crack gage signal being received by the data acquisition system (SPARTAN). The distances between the strands are 0.51 mm (0.02 in.) and 2.03 mm (0.08 in.) for the TK-09-CPA02-005/DP and TK-09-CPC03-003/DP, respectively. The data acquisition system was directly connected with a MTS model 407 controller.

The fatigue precracking was conducted on all the specimens to obtain ideal sharp cracks. The length of fatigue precrack (a_0 ; initial crack length) longer than $b/16$ was achieved following the ASTM E 647. Then, the crack gages were attached on the specimens and connected to the data acquisition system as previously described. The fatigue tests were conducted under sinusoidal cyclic tension-tension loading (Table 2). Two different load ratios, R , of 0.1 and 0.5 were applied to each type of specimen to investigate the effect of load ratio on fatigue crack growth; R = ratio of the minimum to maximum load (P_{min}/P_{max}). The effect of loading frequency on fatigue crack growth was also studied for aluminum 2014-T6 specimens. Additionally, Table 2 shows the initial crack length for each specimen at which the experimental data began to be collected and analyzed.

3. Experimental results and discussion

3.1 Fatigue crack growth

The stress intensity factor, K , characterizes the magnitude of the stress field ahead of an ideally sharp crack in a linear-elastic and isotropic material. For the compact specimen, the stress intensity factor, K , in Mode I (opening mode) can be calculated by the following equation (Dowling 1999):

$$K = F(\alpha) \frac{P}{t\sqrt{b}}; \quad \alpha = \frac{a}{b} \quad (1)$$

where P = magnitude of the applied load; a = crack length; b = width of the specimen; and t = thickness of the specimen. The factor $F(\alpha)$, which is a dimensionless function depending on the geometry and loading configuration for the compact specimen, is as follows (Dowling 1999):

$$F(\alpha) = \frac{(2 + \alpha)}{(1 - \alpha)^{3/2}} (0.886 + 4.64\alpha - 13.32\alpha^2 + 14.72\alpha^3 - 5.6\alpha^4) \quad (a/b \geq 0.2) \quad (2)$$

Since this K concept is based on the LEFM theory, the crack lengths used in this study should satisfy an overall limit on use of the LEFM, which is given in Eq. (3).

$$a, (b - a), h \geq \frac{4}{\pi} \left(\frac{K}{\sigma_o} \right)^2 \quad (\text{LEFM applicable}) \quad (3)$$

where σ_o = yield stress; and h = half the specimen height.

Using the crack gage signals, a plot of voltage vs. number of loading cycles for each specimen tested was made. The data of crack length and number of loading cycles were then obtained from the plot points where the voltage jumped up. Fig. 3 shows the plot of the crack length vs. number of loading cycles for AL1#1. To obtain the crack growth rates, da/dn , from the plot of the crack length vs. number of loading cycles data, the straight-line slopes between the data points were used. The crack growth rate for the interval ending at data point numbered j was then

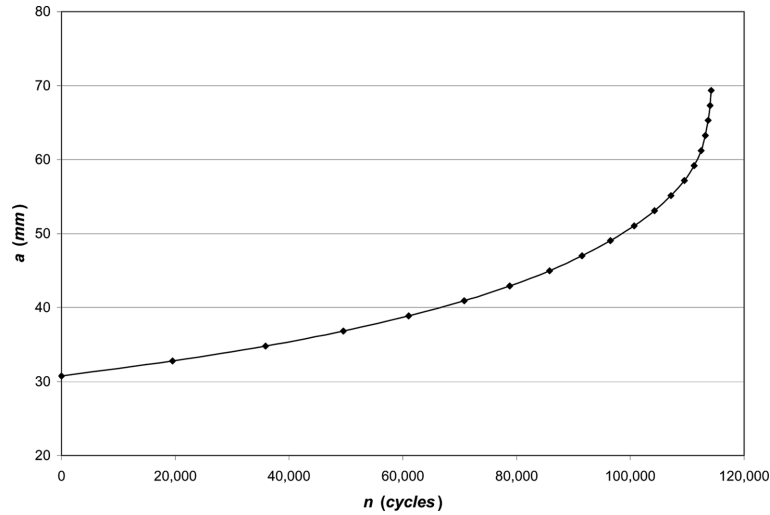


Fig. 3 Plot of crack length vs. loading cycles for AL1#1

$$\left(\frac{da}{dn}\right)_j \approx \left(\frac{\Delta a}{\Delta n}\right)_j = \frac{a_j - a_{j-1}}{n_j - n_{j-1}} \quad (j = 1, 2, 3, \dots) \quad (4)$$

where n = number of loading cycles. The corresponding stress intensity range, ΔK , for the interval was calculated from the average crack length, a_{avg} .

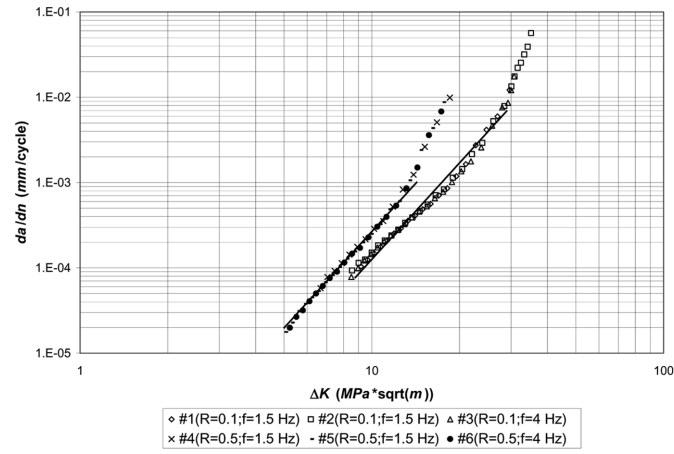
$$a_{avg} = \frac{a_j + a_{j-1}}{2}; \quad \alpha_{avg} = \frac{a_{avg}}{b}; \quad n_{avg} = \frac{n_j + n_{j-1}}{2} \quad (5)$$

$$(\Delta K)_j = \Delta K_{avg} = F(\alpha_{avg}) \frac{\Delta P}{t\sqrt{b}} \quad (6)$$

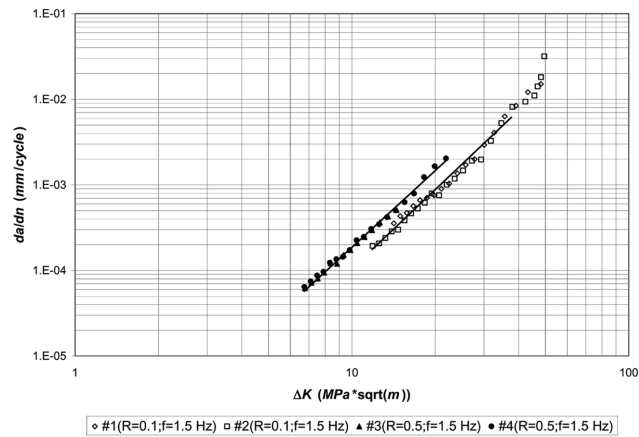
where $\Delta P = P_{max} - P_{min}$. The relationship between da/dn and ΔK for each specimen tested was established and plotted on a log-log scale as shown in Fig. 4.

The effect of cyclic loading frequency on the crack growth rate was established from the results of fatigue tests on aluminum 2014-T6 specimens subjected to two different loading frequencies, f , of 1.5 and 4 Hz. Fig. 4(a) shows that the crack growth rates were not affected by the loading frequencies. It is also shown in Rolfe and Barsom (1977) that there was no effect of cyclic loading frequency on the crack growth rates for ASTM A36 steel under the loading frequencies of 0.1 to 50 Hz. Both of the above results were obtained under a benign room-temperature environment.

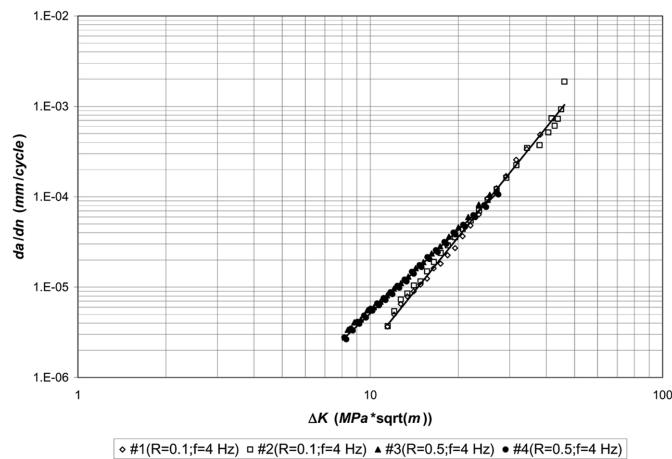
In general, it is known that the effect of R on the crack growth rate is more pronounced for more brittle materials, and variations in R from 0 to 0.2 have little effect on most materials in the mid-growth rate region where the relationship between the crack growth rate and stress intensity range is linear on log-log scale (Dowling 1999). Fig. 4 illustrates that an increase in the load ratio, R , from 0.1 to 0.5 caused the crack growth rates for a given stress intensity range to be larger, especially for the aluminum specimens. Since the data from the specimens that were made of the same material and tested under the same R lay quite close to the single line as shown in Fig. 4, the data were



(a)



(b)



(c)

Fig. 4 Crack growth rate vs. stress intensity range: (a) Aluminum 2014-T6 specimens, (b) Aluminum 7050-T76511 specimens, (c) ASTM A36 Steel specimens

Table 3 Experimentally obtained C and m in the Paris Law

Material	Load ratio, R	Data regions for linear regression		C	m
		ΔK (MPa \sqrt{m})	da/dn ($\times 10^{-6}$ mm/cycle)		
Aluminum 2014-T6	0.1	8.51~28.47	78~7,883	4.15×10^{-8}	3.51
	0.5	5.04~13.90	18~1,238	5.18×10^{-8}	3.72
Aluminum 7050-T76511	0.1	11.88~37.99	194~8,161	1.02×10^{-7}	3.01
	0.5	6.73~21.88	64~2,036	2.36×10^{-7}	2.90
ASTM A36 Steel	0.1	11.46~44.97	3.7~927.0	2.48×10^{-10}	3.98
	0.5	8.16~27.03	2.8~111.4	5.12×10^{-9}	3.03

combined into a group to calculate the experimental constant C and m in the Paris Law (Eq. (7)) for a combination of the material and R .

$$\frac{da}{dn} = C(\Delta K)^m \quad (7)$$

where C , m = material dependent constants. This equation represents a straight line at intermediate values of ΔK on the log-log plot.

The fitted line on the log-log plot of the crack growth rate vs. stress intensity range for each combination of material and R used is also shown in Fig. 4, and the values of C and m from the fitted line are listed in Table 3. The fitted lines lie on the mid-growth rate regions containing the data changing linearly. The data ranges on which the linear regression was conducted are listed in Table 3 as well. The results for aluminum 2014-T6 and 7050-T76511 specimens show that the slope, m , of the fitted line for each material stays fairly constant regardless of R , while the intercept, C , of the fitted line increases with increasing R . However, in the case of ASTM A36 steel, the results show that the slope, m , is not constant for varying R , and the R effect seems much stronger at the low growth rate than at the high growth rate. According to Dowling (1999), mild steel and other relatively low-strength, highly ductile, structural metals exhibit only a weak R effect in the mid-growth rate region, but exhibit a strong R effect in the slow-growth rate region. This fact, as well as using different P_{max} loads (4.90 kN for $R=0.1$ and 6.22 kN for $R=0.5$), may contribute to the results of the current ASTM A36 steel specimens. Several references (Barsom 1971, Crooker 1971, Rolfe and Barsom 1977, Gan and Weertman 1981) show the plots of the crack growth rate vs. stress intensity range for various high-strength aluminum alloys and ferrite-pearlite steels such as aluminum 2014-T6, 7050-T76511, and ASTM A36 steel. The experimental results (Fig. 4) obtained in our study are comparable to the results from these references. A recent fatigue study of aluminum 2024-T3 (Kermanidis and Pantelakis 2001) also shows a range of crack growth rate similar to our results under constant stress amplitudes.

To calculate the values of C and m for various R values, an empirical equation has been introduced by Dowling (1999).

$$C = \frac{C_1}{(1-R)^{m_1(1-\gamma)}}, \quad m = m_1 \quad (8)$$

Table 4 Predicted values of C and m at various R

Load ratio (R)	Aluminum 2014-T6 ($\gamma = 0.90$)		Aluminum 7050-T76511 ($\gamma = 0.52$)		ASTM A36 Steel	
	C	m	C	m	C	m
0	3.99×10^{-8}	3.61	8.83×10^{-8}	2.96	—	—
0.1	4.15×10^{-8}	3.61	1.02×10^{-7}	2.96	2.48×10^{-10}	3.98
0.2	4.34×10^{-8}	3.61	1.21×10^{-7}	2.96	—	—
0.3	4.57×10^{-8}	3.61	1.46×10^{-7}	2.96	—	—
0.4	4.84×10^{-8}	3.61	1.82×10^{-7}	2.96	—	—
0.5	5.18×10^{-8}	3.61	2.36×10^{-7}	2.96	5.12×10^{-9}	3.03
0.6	5.64×10^{-8}	3.61	3.24×10^{-7}	2.96	—	—
0.7	6.28×10^{-8}	3.61	4.87×10^{-7}	2.96	—	—
0.8	7.32×10^{-8}	3.61	8.65×10^{-7}	2.96	—	—
0.9	9.50×10^{-8}	3.61	2.31×10^{-6}	2.96	—	—

- (1) The values of m for aluminum 2014-T6 and 7050-76511 in Table 4 was obtained by averaging the experimentally obtained slope (m) at $R = 0.1$ and $R = 0.5$ listed in Table 3.
- (2) The values of C should be used with units of $\text{MPa}\sqrt{\text{m}}$ and mm/cycle , and those in shaded cells were experimentally obtained.

where C_1 , $m_1 =$ intercept and slope on the log-log plot of the Paris Law for the special case of $R = 0$, respectively; and $\gamma =$ constant for the material. This equation is established by the fact that the straight lines for various R on the log-log plot of the crack growth rate vs. stress intensity range lie quite parallel to each other (Kim and Mubeen 1981, Dennis 1986). Substituting the experimentally obtained values of C and m ($=m_1$) at $R = 0.1$ and $R = 0.5$ for each material into Eq. (8) provided two equations for each material. By solving the two equations with respect to C_1 and γ , the values of C_1 and γ for each material were obtained. In this process, the value of m_1 for each material was assumed to be a constant value by using the average value of the experimentally obtained slopes (m) at $R = 0.1$ and $R = 0.5$. Substituting the obtained values of C_1 , m_1 , and γ for a given material into Eq. (8) then provided an equation to approximately predict the values of C and m at various R . Table 4 shows the predicted values of C and m at various R for each of aluminum 2014-T6 and 7050-T76511. As can be seen in the preceding results, the crack growth rate for a given material is a function of ΔK and R . The value of C in Table 4 represents the effect of R on the crack growth rate. Since the slope, m , for ASTM A36 steel has very different values at $R = 0.1$ and $R = 0.5$ as shown in Table 3, Walker’s equation could not be applied for this material.

3.2 Life estimation of tested specimens

The life for a crack growth can be expressed in terms of the number of cycles and calculated by solving the following equation.

$$n_{if} = n_f - n_i = \int_{n_i}^{n_f} dn = \int_{a_i}^{a_{if}} \left(\frac{dn}{da} \right) da \tag{9}$$

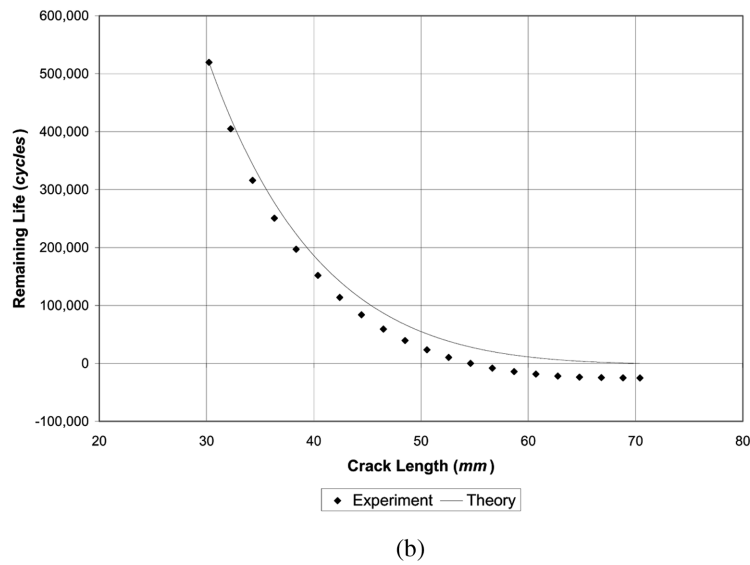
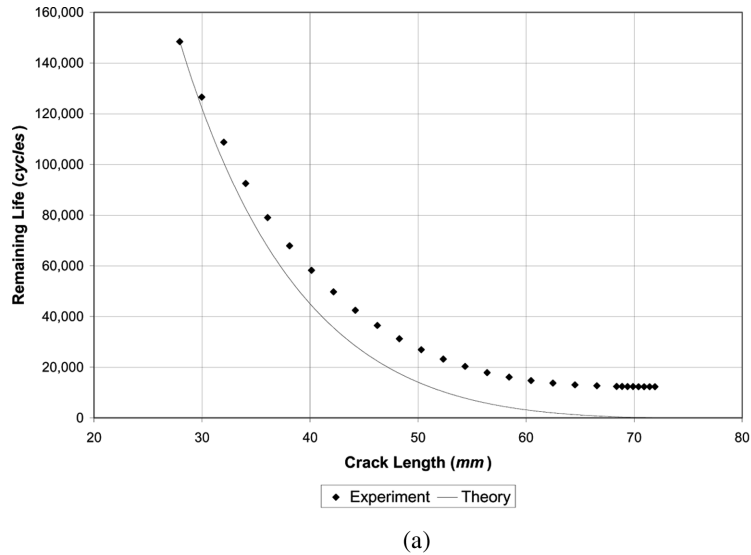


Fig. 5 Remaining life vs. crack length: (a) AL1#2, (b) AL1#5

$$\frac{dn}{da} = \frac{1}{C(\Delta K)^m} \tag{10}$$

The number of cycles, n_{jf} , required for the crack to propagate from an initial crack length, a_i , at cycle number, n_i , to a final crack length, a_f , at cycle number, n_f , can be found by solving Eq. (9). The remaining life of each specimen at a given crack length to a_f was calculated by substituting the corresponding values of C and m for raw data listed in Table 3 into Eq. (9) and was plotted to be compared with its experimental result; this calculated remaining life is presented as theoretical remaining life in Fig. 5, which shows two representative comparisons for the cases of AL1#2 and AL1#5.

As can be seen in Fig. 5, it was found for each specimen that there was discrepancy between the experimental and theoretical remaining life. This is caused by the use of the values of C and m as given in Table 3, which were obtained from an integrated plot of the crack growth rate vs. stress intensity range for a combination of different materials and R values. For AL1#2, the theoretical remaining life at $a_i = 27.94$ mm (1.1 in.) to $a_f = 71.93$ mm (2.832 in.) is about 148,000 cycles, and this is about 12,000 cycles longer than the experimental one. In this case, it can be said that the theoretical remaining life is about 9% higher than the experimental (or real) remaining life for AL1#2. In the other case of AL1#5, the theoretical remaining life at $a_i = 30.23$ mm (1.19 in.) to $a_f = 70.41$ mm (2.772 in.) is about 520,000 cycles, about 25,000 cycles shorter than the experimental value. Therefore, for this specimen, using the theoretical remaining life is about 5% more conservative in predicting the experimental (or real) remaining life. The error in the cases of the other specimens was within the above percentage range.

4. FEM calculation and results

The J -integral is to generalize the strain energy release rate, \mathcal{G} , in case that the nonlinear material behavior is dominant due to the large amount of plasticity in the vicinity of crack tip, to which LEFM can not be applied. By idealizing elastic-plastic behavior as nonlinear-elastic, the J -integral is proved to be able to handle the practical problems occurring beyond the limits of LEFM (Rice 1968). Shih *et al.* (1986) introduced the domain integral method that is relatively simple and accurate to evaluate J numerically with rather coarse finite element meshes. This domain integral in 2-D problem is called the area integral. When the plastic zone is negligibly small (LEFM), the J value is equivalent to the strain energy release rate, \mathcal{G} , and is able to be related to an equivalent value of K under Mode I as follows.

$$K_J = \sqrt{JE} \quad (\text{Plane Stress}) \quad (11)$$

$$K_J = \sqrt{\frac{JE}{1-\nu^2}} \quad (\text{Plane Strain}) \quad (12)$$

where K_J = stress intensity factor estimated by using J value.

The singularity at the crack tip in linear elastic problem can be produced by certain element-node configuration. The 8-node quadrilateral isoparametric element, which is a second-order element, is usually used in 2-D crack problems. The elements around crack tip should be modified to exhibit $1/\sqrt{r}$ singularity, suitable for linear elastic problems. This method of creating singularity in quadratic isoparametric element was introduced in detail by Barsoum (1976). Using a finite element simulation program, ABAQUS, the compact-tension specimens with different crack lengths were modeled to obtain J values at different crack lengths so that these J values were compared with equivalent values of K from Eq. (1). As a result, K_J values agree well with K values from Eq. (1) (Fig. 6), and hence the above approach to create the singular elements is proved to be reliable. The details of this FEM modeling can be found in Choi (2000).

4.1 Simplified FEM models of AVLB sub-components

The simplified 2-D modeling in LEFM standpoint was conducted for three critical sub-

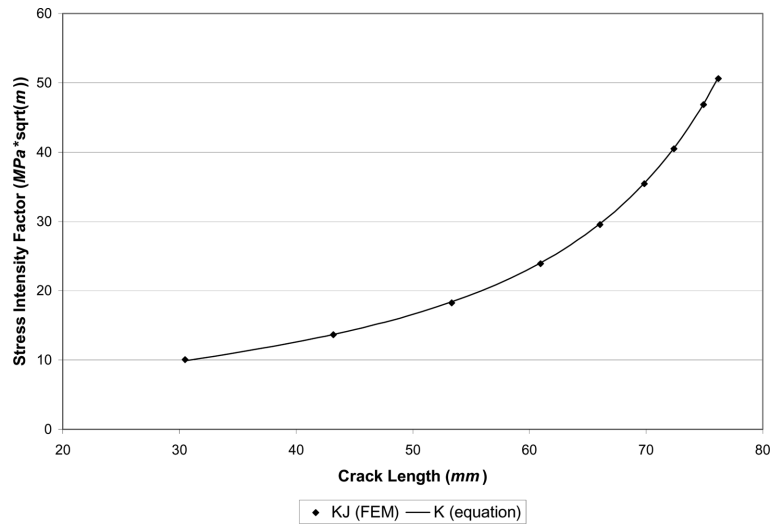


Fig. 6 Stress intensity factor vs. crack length for aluminum 2014-T6 specimen subjected to $P = 5.34$ kN (comparison of K_J and K)

components, which contain a number of rivet-holes. It was assumed in the modeling that the crack initiates from the rivet-hole where the stress concentration takes place, and only the cracked rivet-hole and its adjacent uncracked rivet-holes were considered in the modeling rather than all rivet-holes. Under the plane stress condition, a series of models with different crack lengths was constructed for each component in order to obtain the J values, from which the stress intensity factors were then calculated using Eq. (11); with the $1/\sqrt{r}$ singularity, even though the J values obtained under the plane stress and the plane strain are different from each other, the K_J values converted by using their corresponding equations (Eqs. (11) or (12)) become equal. The materials and geometric dimensions for the modeling were based on the components of the AVL B at WVU. The geometric dimensions of these components are shown in Choi (2000).

4.1.1 Simplified splice doubler angle FEM model

The splice doubler angle, which is made of aluminum 2014-T6, has twelve rivet-holes in a row in both the flange and the web (Figs. 7(a) and (b)). Since the type of stressing the component and the magnitude of load through each rivet-hole were unknown, several assumptions for those were established in the modeling to simulate the stress distribution around the crack tip. In addition to the assumptions, geometric simplifications were adopted in 2-D. The assumptions and simplifications are as follows: (1) The component is subjected to tensile loads; (2) The crack initiates from a rivet-hole in the flange, where the stress concentration occurs. In addition, this crack initiates only at the rivet-hole edge close to the edge of the flange and propagates only toward the edge of the flange (not toward the web); (3) The 2-D simplified model, which is based on the angle L102 mm \times 102 mm \times 6.4 mm (L4 in. \times 4 in. \times 0.25 in.), is 406.4 mm (16 in.) long. Fig. 8(a) shows the dimensions of the simplified model; (4) Three rivet-holes, a cracked middle hole and two uncracked adjacent holes, are included in the model to consider the geometric effect of the adjacent holes on the stress distribution around the cracked hole. The cracked middle hole between two other uncracked holes is centered in the longitudinal direction of the model; (5) The stress of 55.16 MPa

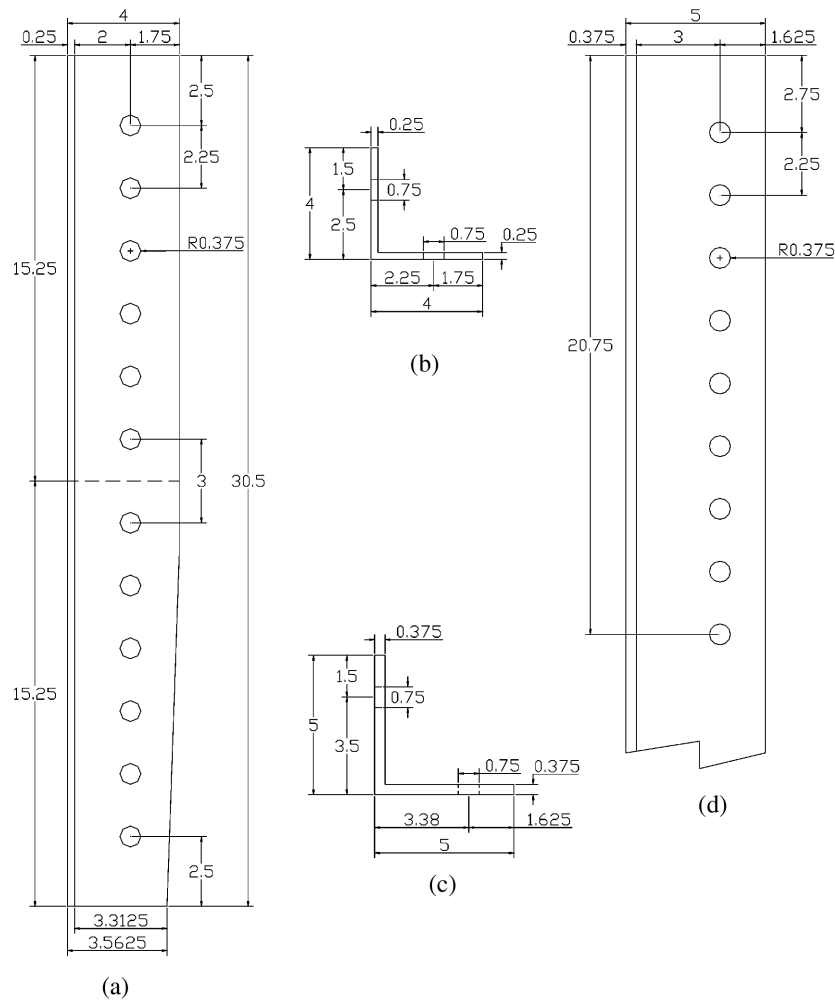


Fig. 7 AVLB components' schematic details (unit of dimension: in.; 1 in. = 25.4 mm): (a) Splice doubler angle flange view, (b) Splice doubler angle front view, (c) Bottom chord front view, (d) Bottom chord flange view

(8,000 psi) is assumed to be uniformly applied to both ends of the component. From the assumption, the applied total load (P) to the flange is calculated such that $33,375 \text{ N} = 55.16 \text{ MPa} \times 95.25 \text{ mm} \times 6.35 \text{ mm}$ ($7,500 \text{ lb} = 8,000 \text{ psi} \times 3.75 \text{ in.} \times 0.25 \text{ in.}$). The load is then applied to the model through the holes; and (6) The stress of 55.16 MPa is uniformly applied to both ends of the web of the model to consider the load applied through the holes in the web.

The model was simulated for three different critical cases of applying the load to the holes in the flange. These three critical cases are pictorially described in Fig. 9. In this figure, the total load is distributed and applied to each hole in terms of stress; $\sigma = P/(2 \cdot r \cdot t)$, where r = radius of the hole and t = thickness of the flange. As a matter of convenience, the cracked middle hole was numbered as #1, the hole below as #2, and the hole above as #3 in the figure.

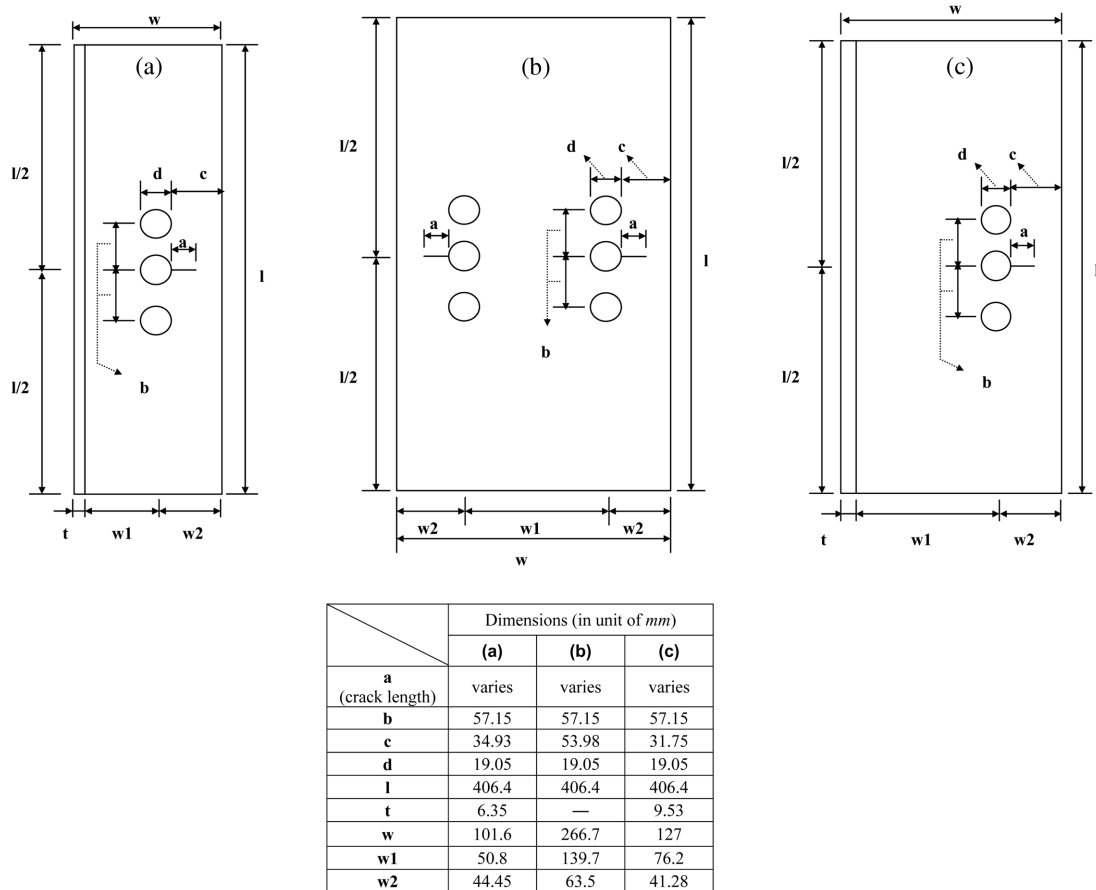


Fig. 8 Dimensions of simplified models: (a) Splice doubler angle (L102 mm \times 102 mm \times 6.4 mm), (b) Splice plate (thickness: 6.4 mm), (c) Bottom chord (L127 mm \times 127 mm \times 9.5 mm)

The simplified models with thirteen different crack lengths were simulated to obtain J values at the different crack lengths. The models were created by using the 8-node quadrilateral isoparametric elements under the plane stress condition. Twelve $1/\sqrt{r}$ singular elements were created adjacent to the crack tip in order to simulate the singular strains and stresses that dominate the vicinity of the crack tip in case of LEFM. Two J -integral domains surrounding the crack tip were set in this modeling. The overall J -integral domain has a size of 16.51 mm (0.65 in.) in the x -direction and 38.1 mm (1.5 in.) in the y -direction. Shown in Fig. 10 is the FE mesh of the simplified splice doubler angle model having a crack length of 12.7 mm (0.5 in.).

The stress intensity factors, K_{Ij} , were calculated from obtained J values by using Eq. (11). The stress intensity factor was then plotted versus crack length for three loading cases as shown in Fig. 13(a). As expected, it can be seen in this figure that Case 1 and Case 3 are presented by the lower and upper boundary plots, while Case 2 by the intermediate plot; considering the superposition principle for LEFM problems, it is reasonable that Case 2 approximately shows the intermediate state between Case 1 and Case 3.

According to the material property reference (Table 1), the plane strain fracture toughness, K_{Ic} ,

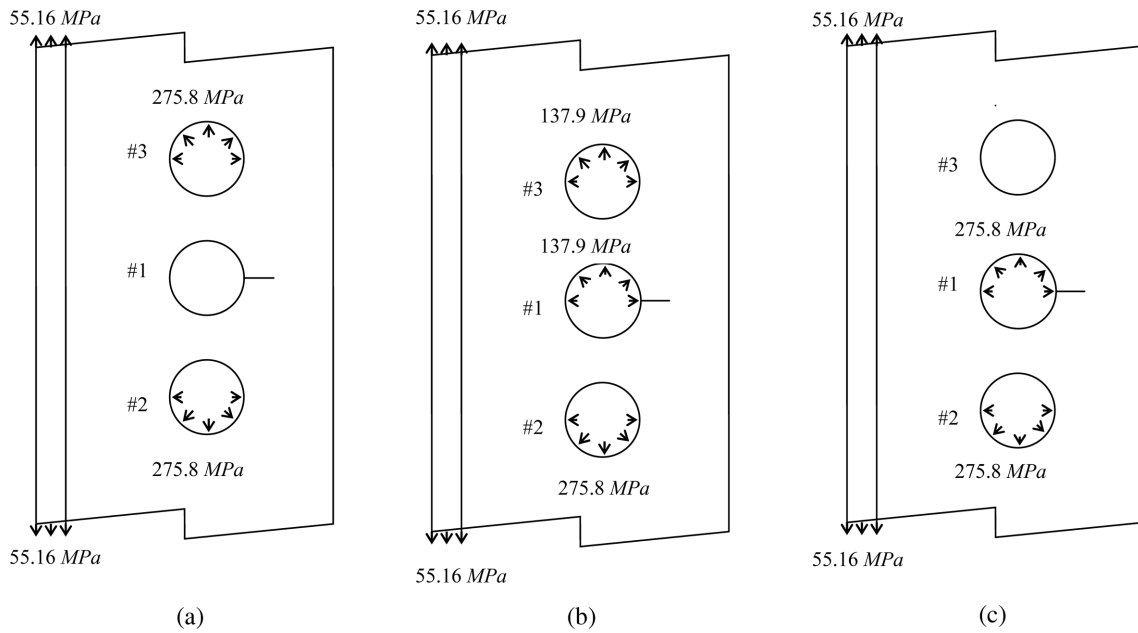


Fig. 9 Three critical cases of applying load to rivet-holes in flange for simplified model of splice doubler angle: (a) Case1, (b) Case2, (c) Case3

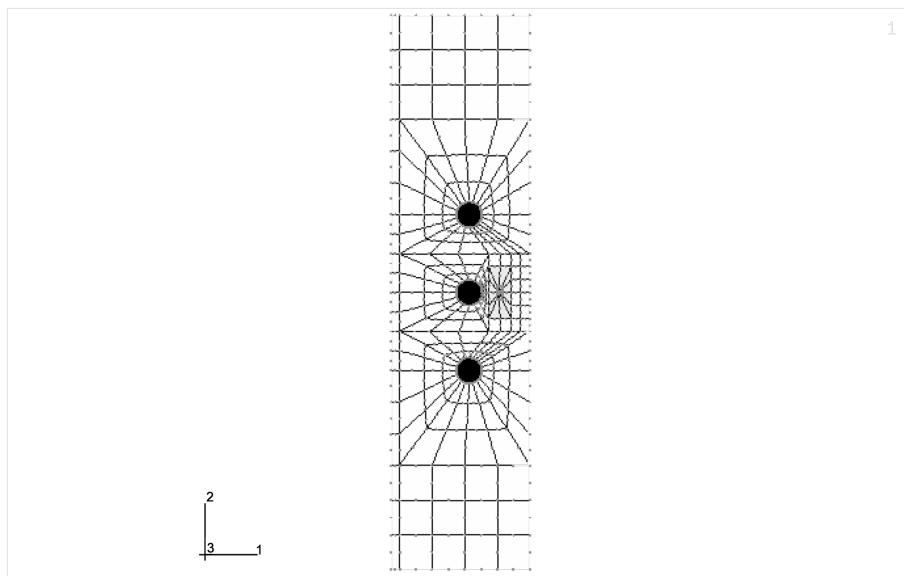


Fig. 10 Simplified splice doubler angle FEM model mesh

which is the smallest fracture toughness value which can be used for other thickness to have a conservative estimation, is about $25 \text{ MPa}\sqrt{\text{m}}$ ($23 \text{ ksi}\sqrt{\text{in.}}$) for aluminum 2014-T6. With this K_{Ic} , the crack length, a_c , which is critical for brittle failure, can be predicted for the simplified splice

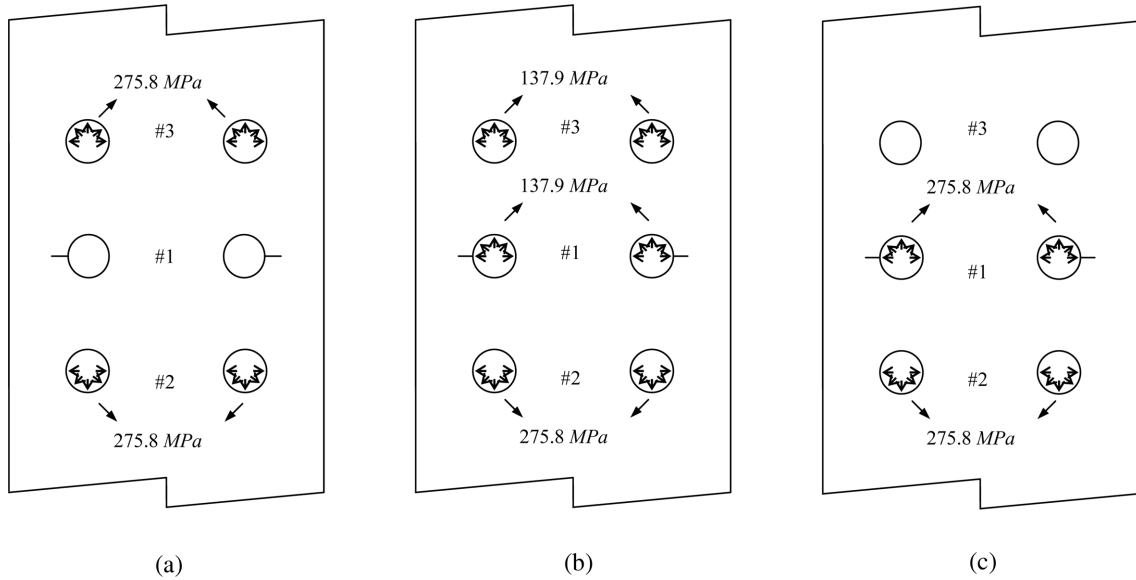


Fig. 11 Three critical cases of applying load to rivet-holes for simplified model of splice plate: (a) Case1, (b) Case2, (c) Case3

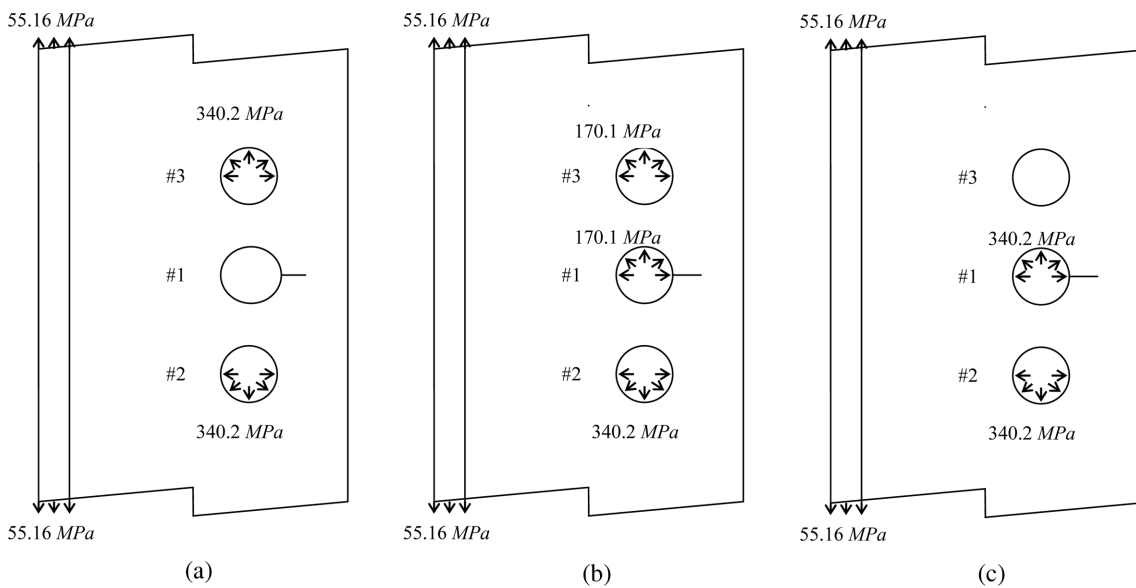
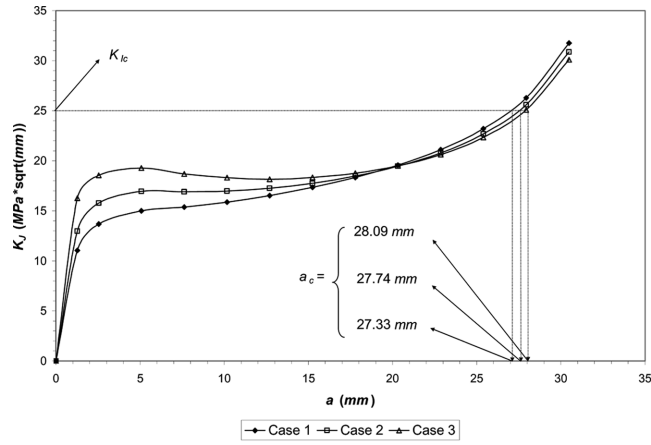
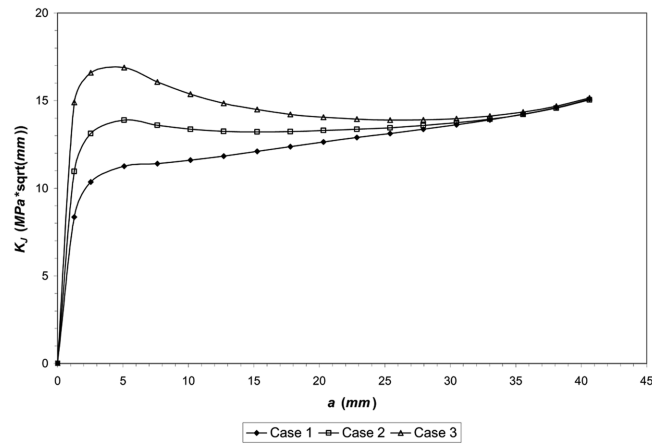


Fig. 12 Three critical cases of applying load to rivet-holes in flange for simplified model of bottom chord: (a) Case1, (b) Case2, (c) Case3

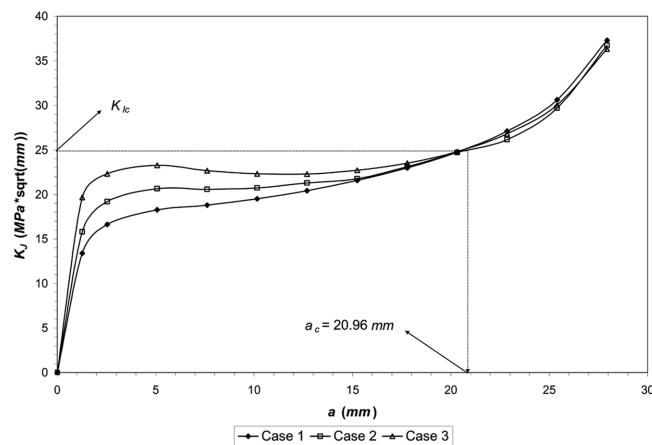
doubler angle model as shown in Fig. 13(a). The critical crack length, a_c , corresponding to the K_{Ic} value of $25 \text{ MPa}\sqrt{\text{m}}$ ($23 \text{ ksi}\sqrt{\text{in.}}$) was determined at about 27.33 mm (1.076 in.), 27.74 mm (1.092 in.), and 28.09 mm (1.106 in.) for Case 1, Case 2, and Case 3, respectively. As a reference, it was reported in Chen and Choi (2004) that for aluminum 2014-T6 specimens, a major jump in AE



(a)



(b)



(c)

Fig. 13 Stress intensity factor vs. crack length for simplified FEM models: (a) Splice doubler angle, (b) Splice plate, (c) Bottom chord

count rate was found when K value at P_{max} reached about $30 \text{ MPa}\sqrt{\text{m}}$ ($27 \text{ ksi}\sqrt{\text{in.}}$) at which point a drastic increase in crack length growth was also observed. This K value is slightly higher than the K_{Ic} for aluminum 2014-T6. Therefore, the critical crack lengths obtained from the K_{Ic} in this study can be considered conservative.

In Fig. 13(a), it can be seen that the level of the stress intensity factors drastically increases in the short crack length region, slightly increases or even decreases in the intermediate crack length region, and then gradually increases as the crack reaches the boundary of the model. The slight increase or decrease of the stress intensity level in the intermediate crack length region would cause the fatigue crack growth rate to decrease in this region.

In addition, since this model is conducted based on LEFM, if a loading level changes by multiplication of a scalar, its K_J value also changes by multiplication of that scalar; its J value changes by multiplication of the square of that scalar. Within the LEFM limit, the K_J at a certain loading level of interest can be thus obtained by multiplying the K_J value by a scalar (multiplier), which is calculated by dividing the loading level of interest by the loading level used in this simulation.

4.1.2 Simplified splice plate FEM model

The splice plate, which is also made of aluminum 2014-T6, has two columns and twelve rows of rivet-holes along the longitudinal direction. Several assumptions and simplifications for loading and geometry were adopted in modeling the component in 2-D: (1) The tensile loads (or stresses) are symmetrically applied to the component with respect to its longitudinal centerline; (2) The crack initiates only at the rivet-hole edge close to the edge of the component and propagates toward the edge of the component (not toward the adjacent rivet-hole). Since the component geometry and loading configuration are symmetric with respect to the longitudinal centerline, it is reasonable to assume that the crack initiates simultaneously from both rivet-holes composing a row and propagates toward both edges of the component at a crack growth rate; (3) Three rows of rivet-holes are considered in this problem so that the geometric effect of the adjacent holes on the stress distribution around a cracked hole can be included in the result. The row of cracked middle holes between two other rows of uncracked holes is centered in the longitudinal direction of the simplified model as shown in Fig. 8(b). The simplified model is 406.4 mm (16 in.) long, 266.7 mm (10.5 in.) wide, and 6.4 mm (0.25 in.) thick; and (4) Since the splice plate is overlapped with the splice doubler angle, the load of 33.36 kN (7,500 lb), which is assumed to be applied to the flange of the simplified splice doubler angle FEM model, is also applied to the half-symmetric splice plate FEM model through the holes.

The simplified models with seventeen different crack lengths were simulated to obtain J values for three different critical cases of applying the load to the holes; these three cases are equivalent to those for the simplified splice doubler angle FEM model and are pictorially described in Fig. 11. The same scheme of creating the elements adjacent to the crack tip, as previously mentioned, was adopted in the modeling. Fig. 13(b) shows the plots of the stress intensity factor vs. crack length for three loading cases.

As can be seen in Fig. 13(b), K_J does not reach the K_{Ic} for aluminum 2014-T6, about $25 \text{ MPa}\sqrt{\text{m}}$ ($23 \text{ ksi}\sqrt{\text{in.}}$), within the considered crack length range of 0 to 40.64 mm (1.6 in.). Therefore, the critical crack length (a_c) can not be obtained within the range. Under the applied load of 33.36 kN (7,500 lb), the K_{Ic} can be reached beyond the crack length of 40.64 mm (1.6 in.), since K_J gradually increases as the crack reaches the boundary of the model.

4.1.3 Simplified bottom chord FEM model

The bottom chord, which is made of aluminum 2014-T6 in the shape of angle, has nine rivet-holes in both the flange and the web (Figs. 7(c) and (d)); the holes in the flange were in a straight row while two holes in one end of the web were offset. The assumptions and simplifications for loading and geometry adopted in modeling the bottom chord in 2-D are the same as those for the splice doubler angle except for the followings: (1) The 2-D simplified model, which is based on the angle L127 mm × 127 mm × 9.5 mm (L5 in. × 5 in. × 0.375 in.), is 406.4 mm (16 in.) long. Fig. 8(c) shows the dimensions of the simplified model; and (2) The stress of 55.16 MPa (8,000 psi) is assumed to be uniformly applied to both ends of the component. From the assumption, the applied total load to the flange is calculated such that 61,744 N = 55.16 MPa × 117.48 mm × 9.53 mm (13,875 lb = 8,000 psi × 4.625 in. × 0.375 in.). The load is then applied to the model through the holes.

Fig. 12 shows three different critical cases of applying the load to the holes for the simplified splice doubler angle FEM model, which has twelve different crack lengths, and Fig. 13(c) shows the plots of the stress intensity factor vs. crack length for three loading cases. Under the given assumption and simplification, the critical crack length (a_c) corresponding to the K_{Ic} of 25 MPa√m (23 ksi√in.) was determined at a value of about 20.96 mm (0.825 in.) for all the loading cases (Fig. 13(c)).

4.2 Life estimation of AVLB components

Using the experimental and FEM results, the crack growth of each AVLB component was estimated in terms of the number of cycles. Eqs. (9) and (10) can be used for the life estimation. Based on the FEM results shown in Fig. 13, the trend equation of the stress intensity factor versus crack length was obtained for each loading case. A typical trend equation of stress intensity factor in terms of crack length for the simplified bottom chord model (Case 2) is shown in Fig. 14; the equations for the other models and loading cases can be found in Choi (2000). Since the FEM

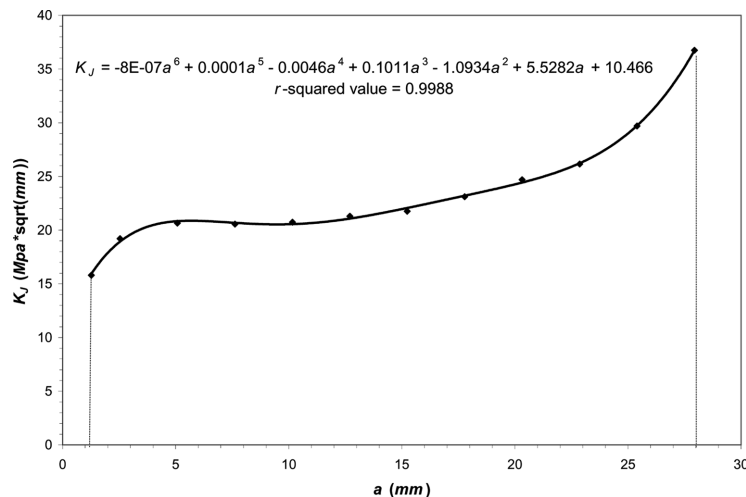
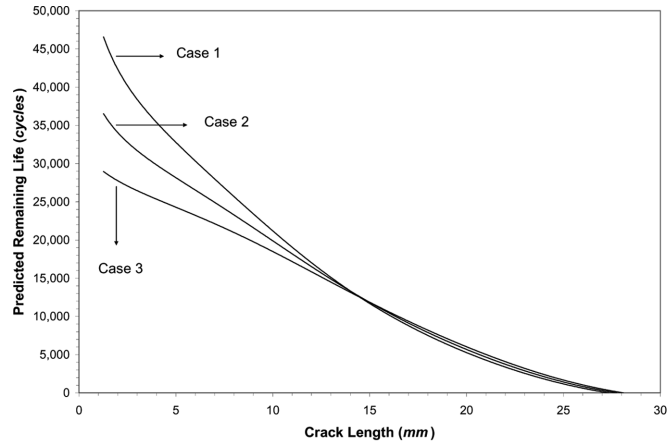
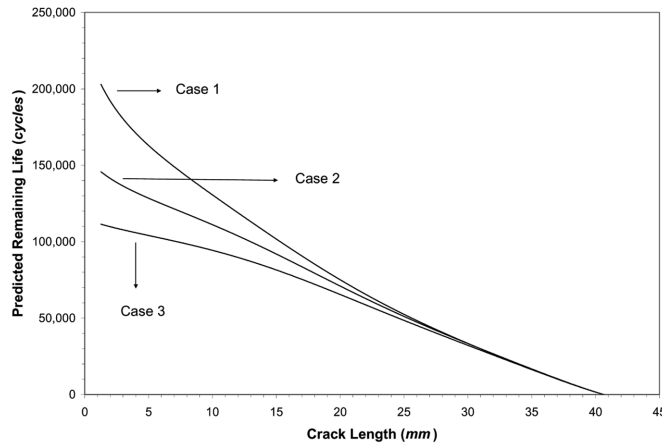


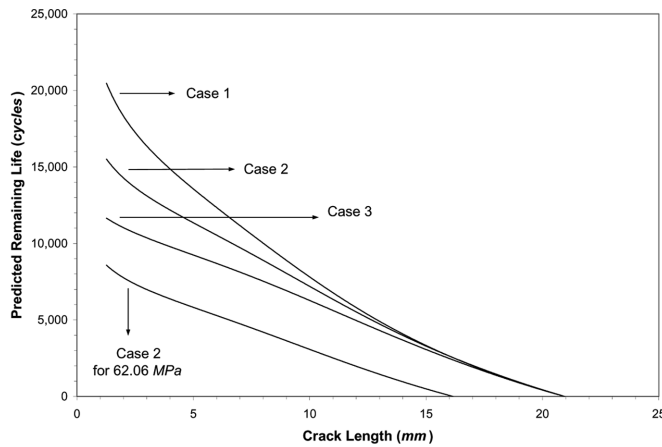
Fig. 14 Fitted curve and equation of stress intensity factor versus crack length for simplified bottom chord FEM model (Case2)



(a)



(b)



(c)

Fig. 15 Predicted remaining life vs. crack length from simplified FEM models: (a) Splice doubler angle, (b) Splice plate, (c) Bottom chord

results were also obtained under the LEFM assumption, the stress intensity range, ΔK_J , can be simply obtained at a certain load ratio, R , as shown in the following equation.

$$\Delta K_J = K_{J, \max} - K_{J, \min} = (1 - R)K_{J, \max} = \left(\frac{1}{R} - 1\right)K_{J, \min} \quad (13)$$

The remaining life of each simplified FEM model from an initial crack length (a_i) of 1.27 mm (0.05 in.) to a final crack length (a_f) was calculated and plotted versus the crack length for each loading case, as shown in Fig. 15. Under $R = 0.1$, the trend equations from the FEM results were substituted into the $K_{J, \max}$ term in Eq. (13), and the obtained ΔK_J equations were then substituted into Eqs. (9) and (10). The $C = 4.15E-8$ and $m = 3.51$, which were experimentally obtained from aluminum 2014-T6 specimens at $R = 0.1$, were used in this calculation as well; since the C and m for aluminum 2014-T6 with the thickness of 6.35 mm (0.25 in.) were not available from the experimental results, the available C and m for the thickness of 9.53 mm (0.375 in.) were instead used in this calculation for the simplified splice doubler angle and splice plate FEM model.

For the life estimation of simplified splice doubler angle FEM model, the critical crack length, a_c , for each loading case was used as its final crack length, a_f . These final crack lengths were 27.33 mm (1.076 in.), 27.74 mm (1.092 in.), and 28.09 mm (1.106 in.) for Case 1, Case 2, and Case 3, respectively. The remaining lives from an initial crack length of 1.27 mm (0.05 in.) to these final crack lengths were predicted as about 46,600, 36,500, and 29,000 cycles for Case 1, Case 2, and Case 3, respectively. For the simplified splice plate FEM model, a crack length of 40.64 mm (1.6 in.), at which the FEM simulation for the model was lastly conducted, was chosen as its final crack length (a_f) for all the loading cases, since the critical crack length (a_c) was not obtained within the range of crack length where the FEM simulation was conducted. The remaining lives from an initial crack length of 1.27 mm (0.05 in.) to a final crack length of 40.64 mm (1.6 in.) were predicted as about 202,900, 145,700, and 111,400 cycles for Case 1, Case 2, and Case 3, respectively. For the simplified bottom chord FEM model, the critical crack length (a_c), which is about 20.96 mm (0.825 in.) for all three loading cases, was used as its final crack length (a_f). The remaining lives from an initial crack length of 1.27 mm (0.05 in.) to the final crack length were predicted as about 20,500, 15,500, and 11,600 cycles for Case 1, Case 2, and Case 3, respectively. If $R = 0.5$ were applied to the calculation following the above procedure, the remaining lives of all the simplified FEM models would be longer than those using $R = 0.1$.

To help understand the life estimation procedure previously explained, an example life estimation is additionally conducted for the simplified bottom chord FEM model. This life estimation is based on the assumption that 6.206 MPa (900 psi) and 62.06 MPa (9,000 psi) are alternately applied to both ends of the component as the fatigue cyclic load ($R = 0.1$), and Case 2 is the governing loading case. Since the assumed maximum stress level is 62.06 MPa (9,000 psi),

$$K_{J, \max} = K_{J, 9000} = 1.125 \times K_{J, 8000} \quad (14)$$

where $K_{J, 9000} = K_J$ equation under the applied stress level of 62.06 MPa (9,000 psi); and $K_{J, 8000} = K_J$ equation under the applied stress level of 55.16 MPa (8,000 psi). Using the $K_{J, 9000}$ equation and the K_{Ic} of 25 MPa \sqrt{m} (23 ksi $\sqrt{in.}$) for aluminum 2014-T6, the critical crack length, a_c , is predicted to be 16.15 mm (0.636 in.). The remaining life from the a_i of 1.27 mm (0.05 in.) to the $a_f (= a_c)$ of 16.15 mm (0.636 in.) is then estimated at about 8,600 cycles (Fig. 15(c)), which is much shorter than the 15,500 cycles obtained using the maximum stress level of 55.16 MPa (8,000 psi).

4.3 FEM discussion

The FEM results were obtained under LEFM assumptions. Therefore, the use of K_I equation should take the LEFM limitations into account. If the K_I values obtained are less than K_{Ic} (or K_c), the FEM results are acceptable. In addition, the K_I equation is established only for the first mode (Mode I; opening mode) of deformation.

Fatigue crack propagation for the real structure is affected by many parameters such as fatigue load level, load-time history, structural geometry, and the environment. Therefore, it is often difficult to predict fatigue crack propagation in service. In the FEM analyses conducted here, some of these parameters were simplified or even ignored, and substituted with some assumptions leading to a fairly tentative result. Even though there are many simplifications, the results provide a first-order estimation for the critical crack length or remaining life of the structural components, which may become useful in a very complicated AVLB damage detection situation. In order to provide more confidence in the estimation, the fatigue tests on the critical AVLB components need to be conducted under real loading conditions in the future.

5. Conclusions

From the laboratory fatigue tests, the relationship between da/dn and ΔK was developed to provide C and m values for each combination of material and load ratio. It was found in the relationships that an increase in R ratio from 0.1 to 0.5 caused the crack growth rate for a given stress intensity range to be larger, especially for the aluminum specimens. Based on the experimentally obtained C and m values, the C and m values at various R were predicted. Using the C and m values, the theoretical (or predicted) remaining lives of the specimens tested were estimated within a margin of error of $\pm 9\%$. In addition, the C and m values obtained here provide the essential data for further fatigue-crack-related studies on the same materials and thicknesses.

The FEM was used to calculate the stress intensity factor as the crack grows in the AVLB structural sub-components. Using the C and m values, together with certain assumptions of loading configuration and loading sequence on the sub-components, the proposed finite element method was found to be a feasible tool for estimating the critical crack lengths and the remaining lives of the AVLB sub-components.

The remaining lives of the sub-components subjected to a cyclic loading with a maximum stress level of 55.16 MPa (8,000 psi) and a load ratio (R) of 0.1 were estimated. Three loading cases were applied to a simplified model of each sub-component to examine the effects of the stress distribution from the rivet-holes. The relationship between K_I and crack length was first established from the FEM results. The remaining life of the sub-component up to the critical crack length was then estimated by using the C , m and K_{Ic} values. From the simplified splice doubler angle and bottom chord FEM models, the remaining life from an initial crack length of 1.27 mm (0.05 in.) to the critical crack length is predicted to be in the ranges of about 29,000 to 46,600 cycles and about 11,600 to 20,500 cycles, respectively. From the simplified splice plate FEM model, the remaining life from an initial crack length of 1.27 mm (0.05 in.) to a final crack length of 40.64 mm (1.6 in.) is predicted to be in the range of about 111,400 to 202,900 cycles.

Acknowledgments

The authors would like to acknowledge the support provided by the U.S. Army/TACOM (Bridge Vibration Sensor System – Phase II, #DAAE07-96-C-X226). Special thanks are extended to Mr. Brian Hornbeck and Mr. Andy Culkin of U.S. Army. The authors also thank the assistance from the Constructed Facilities Center at West Virginia University.

References

- ASM HANDBOOK (1990), *Properties and Selection: Nonferrous Alloys and Special-Purpose Materials*, **2**, ASM International.
- Barsom, J.M. (1971), "Fatigue-crack propagation in steels of various yield strengths", *Transactions of the ASME, J. of Engineering for Industry, Series B.*, **93**(4), November.
- Barsoum, R.S. (1976), "On the use of isoparametric finite elements in linear fracture mechanics", *Int. J. Numer. Meth. Eng.*, **10**, 25-37.
- Chen, H.L. and Choi, J.H. (2004), "Acoustic emission study of fatigue cracks in materials used for AVLB", *J. of Nondestructive Evaluation*, **23**(4), 133-151.
- Chen, H.L. and Fultineer, R.D. (1996), "Study of fatigue cracks in steel bridge components using acoustic emission", *Structural Materials Technology*, An NDT Conference, 317-322.
- Cho, N.K. (1994), *Final Report Preproduction Qualification Test (PPQT) of the Armored Vehicle Launch Bridge (AVLB) MLC 70 Upgrade Program*, Report No. CSTA-7567, U. S. Army Combat System Test Activity, Aberdeen Proving Ground, MD.
- Choi, J.H. (2000), "The fracture analysis and remaining life estimation of the AVLB sub-components", Master Thesis, West Virginia University, Morgantown.
- Clark, Jr. W.G. and Wessel, E.T. (1967), "Interpretation of the fracture behavior of 5456-H321 aluminum with WOL toughness specimens", Scientific Paper 67-1D6-BTLFR-P4, Westinghouse Research Laboratory, Pittsburgh.
- Crooker, T.W. (1971), "Crack propagation in aluminum alloys under high-amplitude cyclic load", Naval Research Laboratory Report 7286, Washington, D. C..
- Dennis, K.R. (1986), "Fatigue crack growth of gun tube steel under spectrum load", Master Thesis, Virginia Polytechnic Institute and State University, Blacksburg, VA.
- Department of the Army (1990), *Technical Manual: Operator's Unit Direct Support and General Support Maintenance for Bridge, Armored Vehicle Launched; Scissoring Type; Class 60 and Class 70 Aluminum; 60 Foot Span; for M48A5 and M60 Launcher; MLC60 and MLC70*, Report No. TM 5-5420-203-14, Headquarters, Department of the Army, Washington, D.C..
- Dhondt, G. (2005), "Cyclic crack propagation at corners and holes", *Fatigue & Fracture of Engineering Materials & Structures*, **28**(1-2), 25-30.
- Dowling, N.E. (1999), *Mechanical Behavior of Materials: Engineering Methods of Deformation, Fracture, and Fatigue*, 2nd ed., Prentice Hall, Upper Saddle River, New Jersey.
- Gan, D. and Weertman, J. (1981), "Crack closure and crack propagation rates in 7050 aluminum", *Engineering Fracture Mechanics*, **15**, 87-106.
- Hamstad, M.A. and McColskey, J.D. (1999), "Detectability of slow crack growth in bridge steels by acoustic emission", *Material Evaluation*, **57**(11), 1165-1174.
- Heo, S.P. and Yang, W.H. (2002), "Prediction of fatigue crack growth path in mechanical joints using a weight function approach", *Fatigue & Fracture of Engineering Materials & Structures*, **25**(10), 985-991.
- Iyer, K., Hu, S.J., Brittan, F.L., Wang, P.C., Hayden, D.B. and Marin, S.P. (2005), "Fatigue of single- and double-rivet self-piercing riveted lap joints", *Fatigue & Fracture of Engineering Materials & Structures*, **28**(11), 997-1007.
- James, L.A. (1972), "The effect of elevated temperature upon the fatigue-crack propagation behavior of two austenitic stainless steels", in *Mechanical Behavior of Materials*, Vol. III, The Society of Materials Science,

- Tokyo, Japan.
- Kermanidis, AL. TH. and Pantelakis, SP. G. (2001), "Fatigue crack growth analysis of 2024 T3 aluminium specimens under aircraft service spectra", *Fatigue & Fracture of Engineering Materials & Structures*, **24**(10), 699-710.
- Kim, K. and Mubeen, A. (1981), "Relation between differential stress intensity factor and crack growth rate in cyclic tension in westerly granite", *Fracture Mechanics Methods for Ceramics, Rocks, and Concrete*, ASTM STP 745, Am. Soc. For Testing and Materials, Philadelphia, PA, 157-168.
- Parry, M., Nordberg, H. and Hertzberg, R.W. (1972), "Fatigue crack propagation in A514 base plate and welded joints", *Welding J.*, **51**(10), October.
- Rice, J.R. (1966), "A path independent integral and the approximate analysis of strain concentration by notches and cracks", *J. Appl. Mech.*, **35**, 379-386.
- Roessle, M.L. and Fatemi, A. (2000), "Strain-controlled fatigue properties of steels and some simple approximations", *Int. J. Fatigue*, **22**(6), 495-511.
- Rolfe, S.T. and Barsom, J.M. (1977), *Fracture and Fatigue Control in Structures : Applications of Fracture Mechanics*, Prentice-Hall Inc., Englewood Cliffs, New Jersey.
- Shih, C.F., Moran, B. and Nakamura, T. (1986), "Energy release rate along a three-dimensional crack front in a thermally stressed body", *Int. J. Fracture*, **30**, 79-102.